DOI: 10.1007/s12541-011-0126-4

Roughness Damage Evolution Due to Wire Saw Process

Egemen Teomete[1,#]

1 Dept. Civil Engineering, Dokuz Eylul University, Kaynaklar Campus Buca, Izmir, Turkey, 35160
Corresponding Author / E-mail: eteomete@gmail.com, TEL: +90-232-4127060, FAX: +90-232-4531192

KEYWORDS: Ceramic, Damage model, Ductile regime machining, Roughness, Wire saw

The wire saw process is widely used for silicon wafer production with high yield and low surface damage in solar cell and microelectronics industries. The wire saw process is used to machine brittle materials in the ductile regime where high yield and low surface damage are desired. The wire saw process is also used to cut concrete and rocks in civil engineering. In this study, an experimental parametric study was conducted by varying process parameters to determine surface roughness damage. Ductile regime material removal by trans-granular failure and brittle fracture by inter-granular failure are observed in electron micrographs of the cut surfaces. A damage model that relates the roughness damage to process parameters was derived. The damage model predicts the roughness damage satisfactorily. The model shows that the roughness damage is proportional to the ratio of feed speed to wire speed. Improvement in the efficiency of the process without increasing the roughness damage can be attained by increasing the feed speed proportionally to wire speed. Wire tension does not affect roughness damage. Roughness damage, however, is affected by properties of the wire. Wires having smaller grit radius and small grit spacing cause less roughness damage.

Manuscript received: May 4, 2010 / Accepted: May 15, 2011

NOMENCLATURE

F_z = Vertical force on a grit
F_{zg} = Force on a single grit
F_{zs} = Total vertical force action on sample
σ_y = Yield stress
R = Grit radius
h = Cut depth for a single particle
V_x = Wire speed
V_z = Feed speed
T = Wire tension
A_p = Projected area of the cut trench
L_o = Cut length of sample
L_g = Distance between cutting particles
D = Width of cut trench
S = Sliding distance
c = Median crack length
ψ = Half of the included angle of the grits
E = Modulus of elasticity of ingot
H = Hardness of the ingot
P = Indentation force
K_c = Fracture toughness of the ingot
w = Distributed wire load on the sample
N = Number of cutting particles in the cut length
α = Wire bow angle

1. Introduction

Silicon wafers used in the solar cell and microelectronics industries can be cut from silicon crystals using inner diameter (ID) saw or wire saw. Wire saw has advantages over ID saw. These advantages are higher productivity, less wafer-surface damage, and lower kerf loss.[1] Moreover, the diameter of wafer that can be sliced by a wire saw is higher than that obtainable by an ID saw.

Wire saws are used to cut sapphire, silicon carbide, lithium niobate, wood, rock, and almost all kinds of ceramics, including foam ceramics.[1-3]

Moller[4] stated that the wire saw process is responsible for 30%

of the total silicon wafer-production cost, which directly affects industry. There is a need to optimize the process by developing models relating process parameters to product quality and process efficiency measures.[4]

Early wire saw processes for wafer production developed in the 1990s consisted of a bare steel wire and abrasive-carrying slurry, resulting in free-abrasive machining using elasto-hydrodynamic forces.[5,6] The abrasive particles can be SiC or diamond. The mean grit size of abrasive particles can be 5 to 30μm with a 30% to 60% volume fraction in the slurry. Average wire diameter is 180 μm, leading to a kerf loss of 200 to 250 μm. The slurry can be water based or oil based. Oil-based slurry causes the wafers to stick to each other, and it is hard to separate them, while removal of the oil from the wafer surface is another problem. Disposal of the oil-based slurry after use is also a problem. Hydrogen gas produced from the interaction of water-based slurry and silicon may cause explosions. However, from an environmental point of view, considering the high amount of slurry disposed of during the process, water-based slurries are generally preferred.[4]

Clark et al.[5] stated that in order to increase the productivity and to be able to cut harder ceramics, diamond-impregnated wire, which leads to fixed-abrasive machining, was developed.

In wire sawing with free abrasives, wire speed is between 5 to 15 m/s and wire tension is 20 to 30 N. The feed into the ingot results in a wire bow so that the wire makes 2^o to 6^o with the horizontal.[6] In the fixed-abrasive machining wire-saw process, the wire speed is lower as material removal is not occurring by hydrodynamic action.

In multi-wire technology, a single wire is winded to a tension control unit and several guide pulleys, which are grooved with constant pitch. Five to seven hundred parallel wires run together and are collected at a take-up spool. The ingot is sliced into hundreds of wafers as it is fed into the wire web. The wafers in solar-cell industry are cut by running the wire in only one direction at a high speed between 5 to 20 m/s, while the wafers in the micro electronics industry are cut by running the wire in both directions with a lower speed (oscillating the wire from one spool to another).[4]

Research on the wire saw process has been ongoing in three main areas: material removal mechanisms, kinematics of wires, and parametric studies between the process inputs and outputs.

Li et al.[7] presented the stresses under an abrasive particle, which is rolling and indenting in a wire saw process. Material removal mechanisms for free-abrasive machining were developed using fracture mechanics and hydrodynamic behavior of slurry by Moller.[4] The material removal rate is defined as a function of power supplied to the abrasive by hydrodynamic effect and the hydrodynamic film properties are calculated using the finite element method which couples Reynold's equation of hydrodynamics with the elasticity equation of wire.[6] Liu et al.[8] stated that the material removal mechanism of bead- impregnated wire-saw cutting of rock is a Hertzian type fracture in which the fracture occurs due to the tensile field behind the sliding bead.

Wei and Kao[9] worked on stiffness analyses of straight and bowed wires under tension. Vibration characteristics of wire with respect to wire speed, tension, and slurry viscosity was investigated. The increase of wire tension and slurry viscosity decreases vibration amplitude and kerf loss, while the wire speed has almost no affect when it is below 25 m/s.[1,10]

Process monitoring of the wire saw for forces, wire speed, feed rate, wire bow, and wire tension was developed by Clark et al..[5] Parametric studies relating process parameters to forces, and surface roughness and wire wear for cutting foam ceramics and wood were conducted by Clark et al..[2] Hardin et al.[11] conducted a parametric study for slicing single crystal SiC with a fixed-abrasive diamond wire, relating wire speed, rocking frequency, and down-feed rate with surface and subsurface damage. Closed-loop diamond- impregnated wire saw cutting of Al_2O_3 and TiC ceramics was studied by Meng et al.[12]

Hardness anisotropy of Lithium Niobate wafers has been investigated using nano-indentation.[13] Bhagavat and Kao[14] determined the direction of approach for three most commonly sliced orientations of silicon considering crystal anisotropy.

Damage evolution due to wire sawing of silicon wafers is of significant interest as the photovoltaic and semiconductor industries have strict tolerances for surface quality. The process-induced damage on brittle materials can be modeled starting with existing damage models of indentation of brittle materials. There exist several models for the failure mechanisms in brittle materials due to indentation.[15-20] Ryu et al. studied indentation on silicon wafer, glass and silicon carbide.[21] Zhao et al. observed the indentation damage modes on ground surface of optical glass.[22]

Ductile regime grinding of brittle materials has been investigated experimentally by different researchers.[23-28] Bifano et al.[24] stated that when the feed is decreased below a certain amount in grinding, a transition of wear mechanism from brittle to ductile mode can be achieved.

In this study, a damage model for wire saw process induced roughness damage is developed. The damage model is based on ductile mode material removal and brittle mode damage, as observed in SEM images of cut surfaces. The damage model predicts the experimentally measured damage successfully. The experimental work is presented in section 2. The model is presented in section 3. The results and discussion of the study are presented in section 4. The conclusions are presented in section 5.

2. Experimental Process

Wire saw experiments were conducted on alumina ceramic. The wire bow angle, wire axial speed, V_x and feed rate, V_z were measured during the wire saw cutting tests. The surface roughness of cut surfaces was also measured. The SEM imaging of cut surfaces was obtained. The equipment used in these measurements and the process parameters are presented in this section.

2.1 Wire Saw Cutting and Wire Bow Angle Measurement

A wire saw machine (Millennium model produced by Diamond Wire Technology in Colorado, Springs) was used in the experiments. This spool-to-spool wire saw machine with rocking motion of the wire can be controlled by the wire speed, V_x, down-

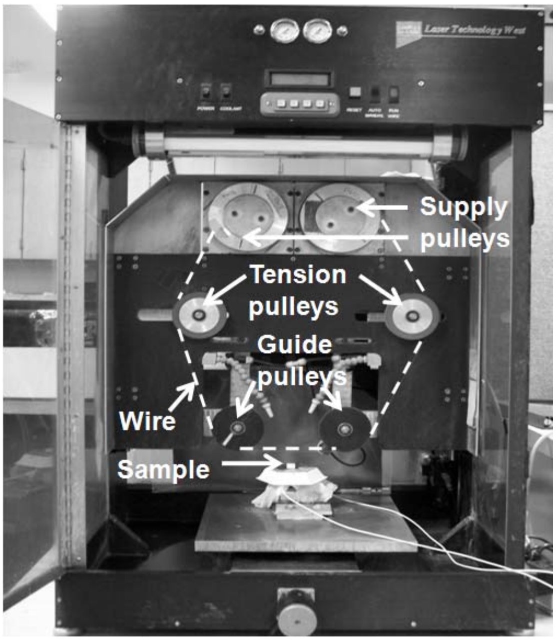

Fig. 1 Single wire, spool-to-spool wire saw machine. The wire track is marked by the dashed line. (DWT Inc., Millennium Model, Colorado, Springs, USA)

feed speed, V_z, and wire tension, T. The tension was controlled by wire tension pulleys powered by air pressure, while the rocking motion was controlled by wire guide pulleys as can be seen in Fig. 1. The cut length of the wire was 300 ft (91.4 m). Thus, at every direction reversal, 300 ft of wire was transferred from one spool to the other.

A coolant consists of water-to-lubricant Sawzit (Product of Synthetic Lubricants, Inc.) ratio of 50/1 was used during cutting tests.

Four different diamond grit coated steel wires were used in the wire saw experiments. The average half-included angle of the grits on DWS2 was ψ=71°. The diamond-grit-coated steel wire DWS3 was a product of Well Diamond Wire Saws Inc. Diamond-grit-coated steel wires DWS4 and DWS5 were products of Saint-Gobain Abrasives Inc. The DWS4 and DWS5 were manufactured by nickel electroplating on steel. The grits were affixed into the electroplated nickel layer, while the core remains intact.

Alumina ceramic samples having tensile strength of σ_{fr}=300 MPa, fracture toughness K_{IC} =4 MPam$^{1/2}$, Young's modulus of E=370 GPa,[29] and hardness of H=22 GPa[20] were used in the cutting tests. The cut length of the samples was between L_o =15~20 mm and the height was H_s =7.1 mm. A group of tests were done with DWS2 with the wire speed varied over V_x=1.3, 1.8, 2.95, 3.5 m/s, the wire tension varied over T=13.3, 17.8, 22.4, 26.7 N, and the down feed varied over V_z=5, 6.35, 10.16 μm/sec. In order to explore the effect of different wires' characteristics on surface quality, twelve tests were done with process parameters V_x=1.35, 2, 3, 4 m/s, V_z=6.35 μm/sec, and T=13.3 N using the wires DWS3, DWS4, and DWS5; four tests were conducted with each wire.

A megapixel digital camera (Kodak Easy Share DX 7630) of 2856 × 2142 pixels was used to measure the wire bow angle seen in Fig. 2. The images of the wire and sample were collected during the test and analyzed using Matlab (Mathworks) to obtain the angle α between the wire and the horizontal. The average of the steady state wire bow angles, α, was attained to the test as the steady state wire bow angle of that test.

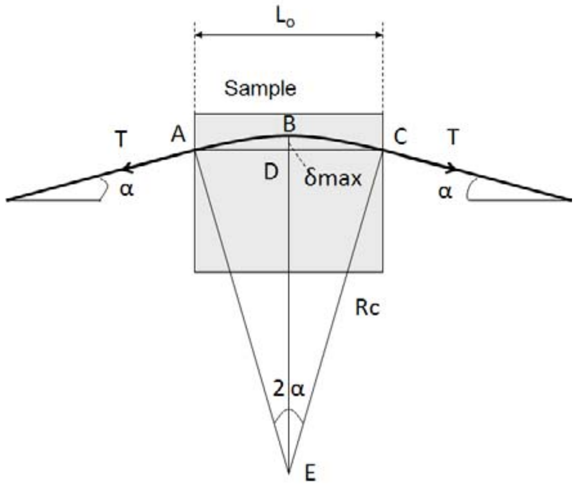

Fig. 2 Wire bow angle in wire saw tests

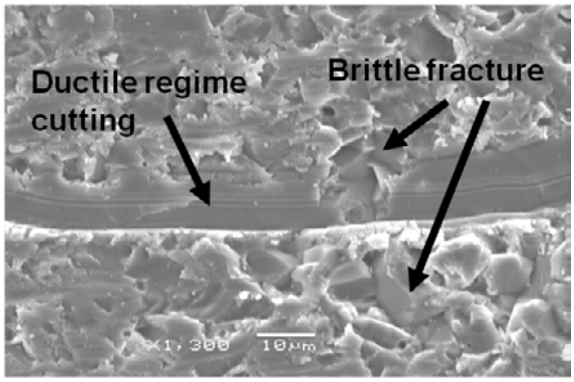

Fig. 3 SEM image of a wire saw cut surface of alumina ceramic (V_x=1.3 m/sec, V_z= 5 μm/sec, T=13 N)

2.2 Surface Roughness Measurements and SEM Imaging

The surface roughness of the cut surfaces were measured by using an optical non-contact profilometer, Zygo New View 6000, manufactured by Zygo Corporation. A 10x lens was used for the measurements. The profilometer had a vertical resolution on the order of 3 nanometer; the resolution in the horizontal plane was 1.1 μm, while the field of view used was 0.7×0.53 mm.

In a stitch measurement, the profilometer takes continuous measurements each 0.7×0.53 mm and stitches them together into one data set. Three stitch measurements, each of 0.7×3 mm dimensions, were applied in the direction of cutting for each sample on the left-middle-right of the cut surface. After the measurements were taken, the data was processed using the software MetroPro Version 8.1.5 developed by Zygo Co. A high pass filtering was applied to remove the surface waviness. Arithmetic average deviation from the centerline (best fit plane) was obtained. The average of three measurements was taken as surface roughness (Ra) of the test.

A Scanning Electron Microscope (SEM), JEOL JSM-606LV, was used to image the cut-surface topology. The SEM images were taken from the lower half of the sample, on the center line of the cut surface. It is seen from the images that the material removal mechanism is the trans-granular failure. Inter-granular failure, in which grain boundary failure results in grain dislodgement in a brittle mode, is also observed. Both mechanisms can be seen in Fig. 3.

3. Roughness Model Derivation

Ductile material removal and brittle fracture is observed in SEM images. The proposed model is shown in Fig. 4. The material removal occurs in a ductile mode as seen in SEM images, while the damage occurs due to median cracking as in Fig. 4. As discussed by Evans and Marshall,[15] removal of plastically deformed material in the cutting zone reduces residual stress. This reduces the tendency of lateral crack formation in brittle materials.

Fu et al.[30] derived the force on a single grit in ductile mode material removal as presented in Eq. (1), where σ_y is yield stress, R is cutting particle radius, and h is cut depth for a single particle.

$$F_z = F_{zg} = \pi\sigma_y Rh \tag{1}$$

The mass continuity of the cutting process gives us Eq. (2).

$$V_z = \frac{d}{dt}\left(\frac{Vol}{A_p}\right) = \frac{d}{dt}\left(\frac{\frac{L_o}{L_g}\times D\times h\times s}{L_o\times D}\right) = \frac{dS}{dt}\left(\frac{h}{L_g}\right) = V_x\left(\frac{h}{L_g}\right) \tag{2}$$

Volume is the total amount of material removed, A_p is the projected area of the cut trench, L_o is the cut length of sample, L_g is the distance between cutting particles, D is width of cut trench that can be taken as diameter of wire, S is sliding distance, V_x is the axial speed of wire, and V_z is the feed of wire.

The force on a single grit, F_{zg}, can be obtained in terms of process parameters by using Eq. (1) and Eq. (2).

$$F_{zg} = \pi\sigma_y RL_g \times \frac{V_z}{V_x} \tag{3}$$

The damage resulting from wire saw cutting is correlated with median crack depth. Lawn et al.[16] derived the median crack length using fracture mechanics principles. The median crack length is presented in Eq. (4). Lawn et al.[16] calibrated the indentation coefficients 0.032 and 0.017 in Eq. (4) using indentation data of soda-lime glass and noted that they are applicable to all brittle materials.

$$c = \left[\left[0.032 + 0.017\times(\cot\psi)^{\frac{2}{3}}\left(\frac{E}{H}\right)^{\frac{1}{2}}\right]\frac{P}{K_c}\right]^{\frac{2}{3}} \tag{4}$$

Inserting Eq. (3) in place of $P=F_{zg}$ in Eq. (4) gives us Eq. (5).

$$c = \left[\left[0.032 + 0.017\times(\cot\psi)^{\frac{2}{3}}\left(\frac{E}{H}\right)^{\frac{1}{2}}\right]\frac{\pi\sigma_y RL_g}{K_c}\right]^{\frac{2}{3}}\left[\frac{V_z}{V_x}\right]^{\frac{2}{3}} \tag{5}$$

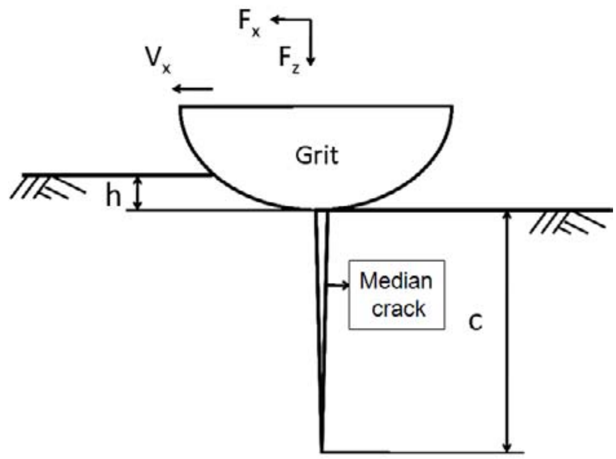

Fig. 4 Wire saw roughness damage model: ductile material removal and brittle fracture

The damage due to the wire saw process is presented in terms of the process parameters in Eq. (5). The damage is a function of the half of the included angle of the grits, ψ; the modulus of elasticity of ingot, E; the hardness of the ingot, H; the fracture toughness of the ingot, K_c; and wire properties, feed speed, and wire speed.

4. Results and Discussion

Decreasing feed rate in grinding below a threshold yields ductile regime grinding of brittle materials.[23-28] In ductile regime machining of brittle materials, the material removal takes place with plastic deformation of the grains.[23,24,26-28,31] While the material removal is in ductile mode, brittle fracture is still observed in ductile regime grinding.[24,28] The material removal and damage formation in the wire saw process is analogous to ductile regime grinding as seen from SEM images of wire saw processed surfaces. A damage model is derived for roughness damage induced by wire saw process. The model is compared to experimental data in Fig. 5. The model has a good performance in predicting roughness damage due to the wire saw process.

The damage model states that if the feed-speed-to-wire-speed ratio (V_z/V_x) is increased, the roughness damage will increase, while if this ratio is kept constant, roughness damage will be constant. The two experiments marked in Fig. 5 have different feed speeds and wire speeds but a very close (V_z/V_x) ratio, and their roughnesses are also very close to each other. In a wire saw process, if efficiency should be increased by increasing the feed speed, in order to keep the level of damage constant, the wire speed should be increased proportionally to the feed speed.

In order to explain the effect of wire tension on roughness damage, the change of forces with wire tension should be considered. The total force and distributed force acting on the sample by the wire due to wire bow and tension is presented in Eq. (6) and Eq. (7), respectively. The total force, F_{zs}, is distributed on the cutting grits as cutting forces per grit, F_{zg}, by Eq. (8). The $N=L_o/L_g$ is the number of cutting particles in the cut length, L_o, and,

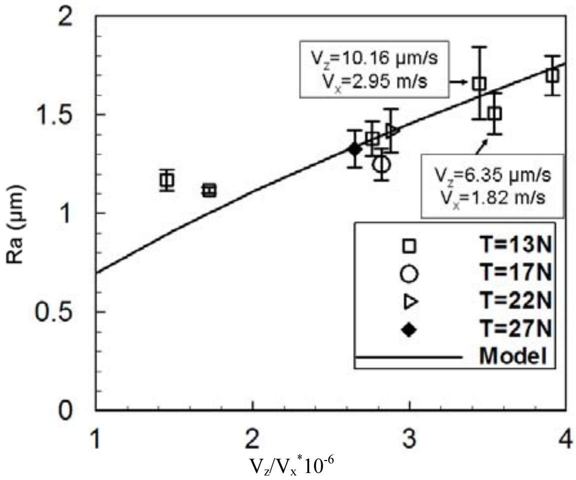

Fig. 5 Comparison of wire saw roughness damage model with respect to experimental results

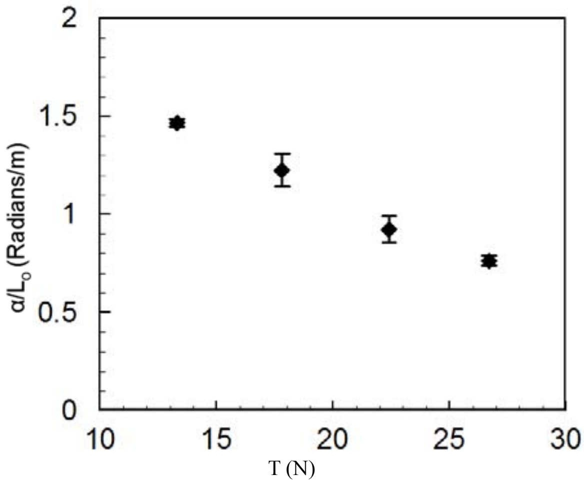

Fig. 6 The variation of normalized wire bow angle by cut length *α/Lo* as a function of wire tension *T* (V_x=1.8 m/sec, V_z= 5 μm/sec)

L_g, is the distance between cutting grits.

$$F_{zs} = 2T\sin\alpha \tag{6}$$

$$w = \frac{2T\sin\alpha}{L_o} \tag{7}$$

$$F_{zg} = \frac{2T\sin\alpha}{N} = \frac{2T\sin\alpha}{L_o}L_g \tag{8}$$

The increase of wire tension, *T*, decreases the wire bow *α* as seen in Fig. 6. As tension, *T*, increases, the wire bow *α* decreases and the distributed load on the sample *w*, remains constant due to Eq. (7), as seen in Fig. 7. The increase of tension, *T*, decreases the bow angle *α* and the force on a single grit, F_{zg}, remains constant due to Eq. (8); thus, the surface roughness does not change with respect to tension, *T*, as seen in Fig. 8. The surface roughness is independent of tension.

The damage model relates the roughness damage with wire properties approximately, as in Eq. (9). The roughness is expected to increase with the increase in the radius, *R*, of abrasive grits and

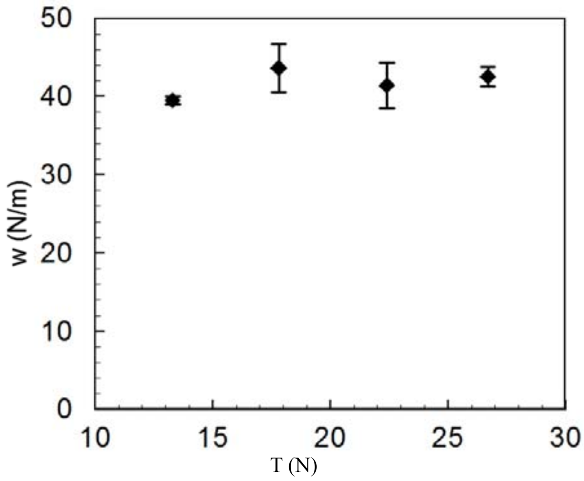

Fig. 7 Variation of distributed load w as a function of wire tension T (V_x =1.8 m/sec, V_z = 5 μm/sec)

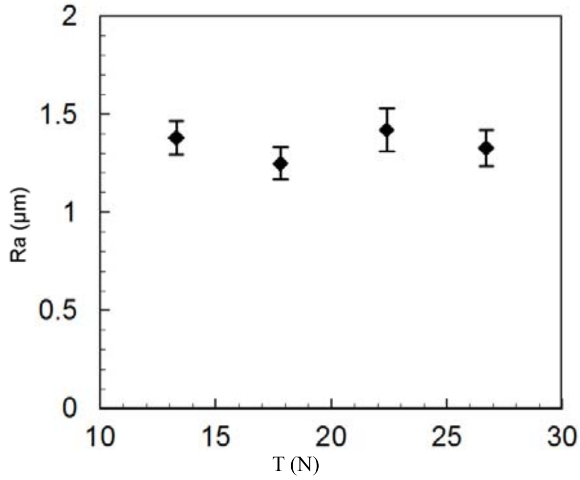

Fig. 8 Variation of surface roughness with respect to wire tension T (V_x =1.8 m/sec, V_z = 5 μm/sec)

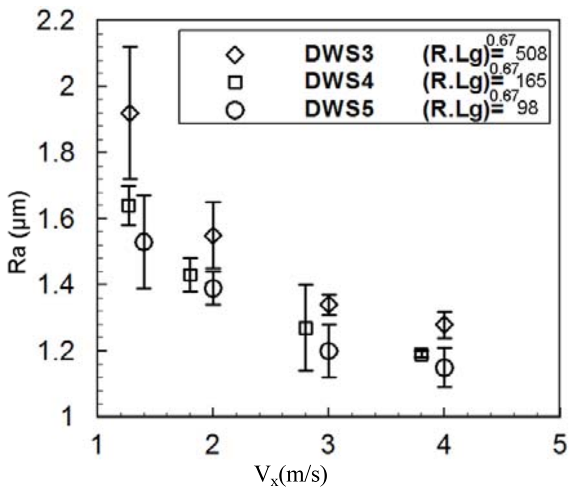

Fig. 9 Variation of surface roughness as a function of wire speed V_x. The tests were carried out with 3 different wires. (V_z = 6.35 μm/sec, T=13N)

the spacing between the abrasive grits, L_g.

$$c \sim (R\times L_g)^{2/3} \tag{9}$$

Four roughness tests with different wire speeds but the same feed speed and tension were done with three different wires. The roughness versus wire speed for each wire is presented in Fig. 9. For the same wire speed, the increase of $(R.L_g)^{0.6}$ yields a higher roughness as seen in Fig. 9. Thus, the prediction of the model about the increase of roughness with grit radius and spacing is verified experimentally.

5. Conclusions

Wire saw process is widely used to slice brittle materials including silicon wafers in semi-conductor and photo-voltaic industries; almost all kinds of ceramics in different engineering applications; concrete and rocks in civil engineering with high yield and low surface damage. The surface damage occurred due to wire saw process decreases the quality of the cut surface and has to be removed by post processes including grinding, and polishing which increase the production cost. In this study an experimental parametric work was conducted for wire saw process with different process parameters. The process induced roughness damage is modeled according to direct observations on the cut surfaces obtained by the process. The results obtained in this study are presented below.

1. The SEM images of the cut surfaces showed that the material removal occurs in the ductile mode, while there is brittle fracture, which is analogous to the ductile regime grinding of brittle materials.

2. In the literature, there has not been an analytical roughness damage model relating the process parameters with the damage for wire saw process.

A roughness damage model relating process parameters to the wire-saw induced roughness damage was derived. The mode of ductile regime cutting and brittle fracture damage on the cut surfaces observed by SEM, have one to one correspondence in the damage model.

Experimental study validated the derived model. The damage model in this work is a contribution to the science and technology as being the only analytical roughness damage model for wire saw process.

3. The model states that the roughness damage is proportional to the ratio of feed speed to wire speed. If the efficiency of the process should be increased without increasing the roughness damage, the feed speed should be increased proportionally with respect to wire speed.

4. Wire tension does not affect surface quality. There is no need to apply high wire tension which will decrease the life of the wire.

5. Wire properties have a marked effect on roughness damage. Wires with smaller grit radius and spacing lead to smaller roughness damage. Wires of high grit density with small grits are beneficial for surface quality.

The results of the damage model can be directly used by the engineers and technicians working on the wire saw process in the industry.

ACKNOWLEDGEMENT

This work is supported by US-National Science Foundation NSF. This work is a part of the author's PhD study in Iowa State University, Iowa, USA.

REFERENCES

1. Zhu, L. and Kao, I., "Galerkin Based Modal Analysis on the Vibration of Wire-Slurry System in Wafer Slicing Using a Wiresaw," Journal of Sound and Vibration, Vol. 283, No. 3-5, pp. 589-620, 2005.
2. Clark, W. I., Shih, A. J., Lemaster, R. L. and McSpadden, S. B., "Fixed Abrasive Diamond Wire Machining–Part II: Experiment Design and Results," International Journal of Machine Tools and Manufacture, Vol. 43, No. 5, pp. 533-542, 2003.
3. Ge, P. Q., Zhang, L., Gao, W. and Liu, Z. C., "Development of Endless Diamond Wire Saw and Sawing Experiments," Materials Science Forum, Vol. 471-472, pp. 481-484, 2004.
4. Moller, H. J., "Basic Mechanisms and Models of Multi–Wire Sawing," Advanced Engineering Materials, Vol. 6, No. 7, pp. 501-513, 2004.
5. Clark, W. I., Shih, A. J., Hardin, C. W., Lemaster, R. L. and McSpadden, S. B., "Fixed Abrasive Diamond Wire Machining–Part I: Process Monitoring and Wire Tension Force," International Journal of Machine Tools and Manufacture, Vol. 43, No. 5, pp. 523-532, 2003.
6. Bhagavat, M., Prasad, V. and Kao, I., "Elasto-Hydrodynamic Interaction in the Free Abrasive Wafer Slicing Using a Wiresaw: Modeling and Finite Element Analysis," Journal of Tribology Transactions of the ASME, Vol. 122, No. 2, pp. 394-404, 2000.
7. Li, J., Kao, I. and Prasad, V., "Modeling Stresses of Contacts in Wire Saw Slicing of Polycrystalline and Crystalline Ingots: Application to Silicon Wafer Production," Journal of Electronic Packaging, Vol. 120, No. 2, pp. 123-128, 1998.
8. Liu, B. C., Zhang, Z. P. and Sun, Y. H., "Sawing Trajectory and Mechanism of Diamond Wire Saw," Key Engineering Materials, Vol. 259-260, pp. 395-400, 2004.
9. Wei, S. and Kao, I., "Analysis of Stiffness Control and Vibration of Wire in Wiresaw Manufacturing Process," Proceeding of ASME Manufacturing Science and Engineering Division, pp. 813-818, 1998.
10. Wei, S. and Kao, I., "Vibration Analysis of Wire and Frequency Response in the Modern Wiresaw Manufacturing Process," Journal of Sound and Vibration, Vol. 231, No. 5, pp. 1383-1395, 2000.
11. Hardin, C. W., Qu, J. and Shih, A. J., "Fixed Abrasive Diamond Wire Saw Slicing of Single-Crystal Silicon Carbide Wafers," Materials and Manufacturing Processes, Vol. 19, No. 2, pp. 355-367, 2004.

12. Meng, J. F., Li, J. F., Ge, P. Q. and Zhou, R., "Research on Endless Wire Saw Cutting of Al_2O_3/TiC Ceramics," Key Engineering Materials, Vol. 315-316, pp. 571-574, 2006.

13. Bhagavat, S. and Kao, I., "Nanoindentation of Lithium Niobate: Hardness Anisotropy and Pop-in Phenomenon," Materials Science and Engineering: A, Vol. 393, No. 1-2, pp. 327-331, 2005.

14. Bhagavat, S. and Kao, I., "Theoretical Analysis on the Effects of Crystal Anisotropy on Wiresawing Process and Application to Wafer Slicing," Int. J. Machine Tools and Manufacture, Vol. 46, No. 5, pp. 531-541, 2006.

15. Evans, A. G. and Marshall, D. B., "Wear Mechanisms in Ceramics," Fundamentals of Friction and Wear of Materials, pp. 439-449, 1980.

16. Lawn, B. R., Evans, A. G. and Marshall, D. B., "Elastic/Plastic Indentation Damage in Ceramics: The Median/Radial Crack System," Journal of the American Ceramic Society, Vol. 63, No. 9-10, pp. 574-581, 1980.

17. Marshall, D. B., Lawn, B. R. and Evans, A. G., "Elastic/Plastic Indentation Damage in Ceramics: The Lateral Crack System," Journal of the American Ceramic Society, Vol. 65, No. 11, pp. 561-566, 1982.

18. Chiang, S. S., Marshall, D. B. and Evans, A. G., "The Response of Solids to Elastic/Plastic Indentation. I. Stresses and Residual Stresses," Journal of Applied Physics, Vol. 53, No. 1, pp. 298-311, 1982.

19. Chiang, S. S., Marshall, D. B. and Evans, A. G., "The Response of Solids to Elastic/Plastic Indentation. II. Fracture Initiation," Journal of Applied Physics, Vol. 53, No. 1, pp. 312-317, 1982.

20. Cook, R. F. and Pharr, G. M., "Direct Observation and Analysis of Indentation Cracking in Glasses and Ceramics," Journal of the American Ceramic Society, Vol. 73, No. 4, pp. 787-817, 1990.

21. Ryu, R. H., Lim, S. H., Jeong, J. I., Shin, D. H., Jang, S. Y., Yim, H. J. and Lee, K. S., "Theoretical and Experimental Analysis of Material Deformation by Microcontact," Int. J. Precis. Eng. Manuf., Vol. 10, No. 2, pp. 111-116, 2009.

22. Zhao, Q., Chen, J., Huang, H. and Fang, X., "Grinding Damage of BK7 using Copper-Resin Bond Coarse-Grained Diamond Wheel," Int. J. Precis. Eng. Manuf., Vol. 12, No. 1, pp. 5-13, 2011.

23. Yoshioka, J., Hashimoto, F., Miyashita, M., Kanai, A., Abo, T. and Daito, M., "Ultraprecision Grinding Technology for Brittle Materials: Application to Surface and Centerless Grinding Processes," Milton C. Shaw Grinding Symposium, ASME Production Engineering Division, Vol. 16, pp. 209-227, 1985.

24. Bifano, T. G., Dow, T. A. and Scattergood, R. O., "Ductile-Regime Grinding: a New Technology for Machining Brittle Materials," Journal of Engineering for Industry, Vol. 113, No. 2, pp. 184-189, 1991.

25. Young, H. T., Liao, H. T. and Huang, H. Y., "Novel Method to Investigate the Critical Depth of Cut of Ground Silicon Wafer," Journal of Materials Processing Technology, Vol. 182, No. 1-3, pp. 157-162, 2007.

26. Ngoi, B. K. A. and Sreejith, P. S., "Ductile Regime Finish Machining - A Review," International Journal of Advanced Manufacturing Technology, Vol. 16, No. 8, pp. 547-550, 2000.

27. Yin, L., Spowage, A. C., Ramesh, K., Huang, H., Pickering, J. P. and Vancoille, E. Y. J., "Influence of Microstructure on Ultraprecision Grinding of Cemented Carbides," International Journal of Machine Tools and Manufacture, Vol. 44, No. 5, pp. 533-543, 2004.

28. Kim, J. D. and Nam, S. R., "Ductile Regime Grinding of Ferrite with Variation of Grain Size by a Piezoelectric-driven Micropositioning Grinding Table," Proc. Instn. Mech. Engrs. Part B: Journal of Engineering Manufacture, Vol. 211, No. 6, pp. 487-493, 1997.

29. Material Property Data, http://www.matweb.com/index.aspx

30. Fu, G., Chandra, A., Guha, S. and Subhash, G., "A Plasticity-based Model of Material Removal in Chemical-Mechanical Polishing (CMP)," IEEE Transactions on Semiconductor Manufacturing, Vol. 14, No. 4, pp. 406-417, 2001.

31. Huang, C., Zhu, H., Lu, X., Li, Q. and Che, C., "Transition Mechanism From Brittle Fracture to Ductile Shear When Machining Brittle Materials with an Abrasive Waterjet," Int. J. Precis. Eng. Manuf., Vol. 9, No. 2, pp. 11-17, 2008.